JOURNAL OF GEOPHYSICAL RESEARCH, VOL. 113, A11205, doi:10.1029/2008JA013444, 2008

Oscillation of Saturn's southern auroral oval

J. D. Nichols,[1,2] J. T. Clarke,[1] S. W. H. Cowley,[2] J. Duval,[1] A. J. Farmer,[3] J.-C. Gérard,[4] D. Grodent,[4] and S. Wannawichian[1]

Received 31 May 2008; revised 26 July 2008; accepted 7 August 2008; published 7 November 2008.

[1] Near-planetary-period oscillations in the Cassini plasma and magnetic field data have been observed throughout Saturn's magnetosphere despite the fact that Saturn's internal magnetic field is apparently highly axisymmetric. In addition, the period of the Saturn kilometric radiation has been shown to vary over time. In this paper we present results from the recent Hubble Space Telescope observations of Saturn's southern ultraviolet auroral emission. We show that the center of the auroral oval oscillates with period 10.76 h ± 0.15 h for both January 2007 and February 2008, i.e., close to the periods determined for oscillations in other magnetospheric phenomena. The motion of the oval center is described for 2007 by an ellipse with semimajor axis ∼1.4° ± 0.3° oriented toward ∼09–21 h LT, eccentricity ∼0.93, and center offset from the spin axis by ∼1.8° toward ∼04 h LT. For 2008 the oscillation is consistent with an ellipse with semimajor axis ∼2.2° ± 0.3° oriented toward ∼09–21 h LT, eccentricity ∼0.99, and a center offset from the spin axis by ∼2.2° toward ∼03 h LT. The motion of the auroral oval is thus highly elliptical in both cases, and the major oscillation axis is oriented toward prenoon/premidnight. This result places an independent constraint on the magnitude of the planet's dipole tilt and may also indicate the presence of an external current system that imposes an asymmetry in the ionospheric field modulated close to the planetary period.

Citation: Nichols, J. D., J. T. Clarke, S. W. H. Cowley, J. Duval, A. J. Farmer, J.-C. Gérard, D. Grodent, and S. Wannawichian (2008), Oscillation of Saturn's southern auroral oval, *J. Geophys. Res.*, *113*, A11205, doi:10.1029/2008JA013444.

1. Introduction

[2] The intrinsic magnetic field of a planet is thought to be generated deep within the planetary interior, such that the rotation period of the magnetic field is generally taken to represent the internal rotation period of the planet. However, Saturn's planetary magnetic field is found to be highly axisymmetric (i.e., rotationally symmetric about the spin axis), rendering direct measurement of the rotation period problematic [*Smith et al.*, 1980; *Dougherty et al.*, 2005]. In spite of this, oscillations near the planetary period have been observed in the magnetic field and plasma data throughout all explored regions of Saturn's magnetosphere and numerous attempts to quantify these have been made [*Espinosa and Dougherty*, 2000; *Clarke et al.*, 2006; *Cowley et al.*, 2006; *Giampieri et al.*, 2006; *Carbary et al.*, 2007a, 2007b, 2007c; *Southwood and Kivelson*, 2007], although the relation to the rotation of Saturn's deep interior is unclear at present. The periodic Saturn kilometric radiation (SKR) was originally thought to be a reasonable proxy for the rotation of the magnetic field, since it is emitted by charged particles whose motion is governed by the magnetic field, and the Voyager-era SKR period of ∼10.66 h [*Desch and Kaiser*, 1981] became the accepted IAU value for the rotation of Saturn's deep interior. However, the SKR period has since been shown to vary over timescales of months to years [*Galopeau and Lecacheux*, 2000; *Gurnett et al.*, 2005; *Kurth et al.*, 2007, 2008], such that significantly longer periods are currently observed, e.g., ∼10.82 h as measured by Cassini in January 2007 [*Kurth et al.*, 2008]. The variability of the SKR period probably results from modulation by external processes, such as corotating magnetospheric convection [*Dessler et al.*, 1981; *Hill et al.*, 1981; *Gurnett et al.*, 2007; *Goldreich and Farmer*, 2007]. In these models the nonaxisymmetric production and outflow of plasma from the moons (mainly Enceladus) and rings causes the period to "slip" with respect to the planet. The SKR period has also been shown to be correlated with the speed of the solar wind at Saturn, although the cause of this modulation is yet to be determined [*Zarka et al.*, 2007].

[3] The January 2007 SKR period of ∼10.82 h is essentially consistent with the magnetic field oscillations near the planetary period that are typically observed within Saturn's magnetosphere, an example of which is shown in Figure 1. These particular data were obtained by the Cassini magnetic field investigation over the interval from 1200 UT on 13 January to 1200 UT on 15 January 2007, thus during the Saturn HST campaign, when the spacecraft was located in

[1]Center for Space Physics, Boston University, Boston, Massachusetts, USA.
[2]Department of Physics and Astronomy, University of Leicester, Leicester, UK.
[3]Harvard-Smithsonian Center for Astrophysics, Harvard University, Cambridge, Massachusetts, USA.
[4]Institut d'Astrophysique et de Géophysique, Université de Liège, Liege, Belgium.

0148-0227/08/2008JA013444$09.00

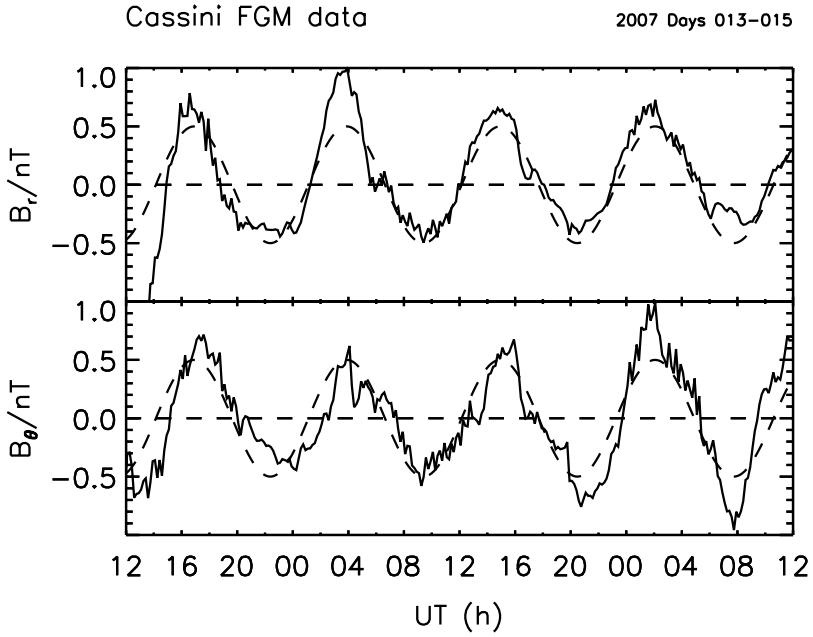

Figure 1. An example of the oscillation observed in Saturn's magnetosphere by the Cassini magnetometer. These data were obtained over the interval from 1200 UT on 13 January to 1200 UT on 15 January 2007. The solid lines show the (top) radial and (bottom) colatitudinal components of the field, while the dashed line shows how a rotating sinusoidal signal with a period of 10.815 h would be observed by Cassini.

the southern dawn magnetosphere at radial distances between ∼20 and ∼14 R_S. The "Cassini" model of the internal planetary field [*Dougherty et al.*, 2005] has been subtracted, and a high-pass filter with a cutoff at 20 h has been applied in order to center the oscillation about zero. The solid lines show the radial (top) and colatitudinal (bottom) components of the field, the latter referenced to the planet's spin axis, while the dashed line shows how a rotating sinusoidal signal with a period of 10.815 h would be observed by Cassini, taking account of the azimuthal motion of the spacecraft [*Cowley et al.*, 2006]. Recently, a relatively small value of ∼10.54 h for the rotation period of the deep interior has been derived from Cassini gravitational data [*Anderson and Schubert*, 2007]. The rotation period of Saturn's interior is thus not well determined.

[4] As for the planetary period, considerable debate is taking place about the nature of the planetary magnetic field. While measurements of the near-planetary field indicate a dipole tilt of ∼1° or less [*Smith et al.*, 1980], such that the field is near-axisymmetric as indicated above, measurements at large distances suggest much larger tilts of up to ∼10° [*Khurana et al.*, 2007], which are thus most likely due to the presence of a variable rotating external current system such as that associated with the SKR modulation. One independent way to assess the asymmetry in the planetary field is to examine the motion of the auroral oval over the planetary period, since a tilt in the dipole relative to the spin axis will cause the center of the oval to rotate with the planet as observed at both Earth and Jupiter [*Grodent et al.*, 2003]. Small motions of the oval can also be caused by a rotating external current system, but the effects of the latter are minimized in the ionosphere where the auroras are formed, since the field there is clearly dominated by the internal planetary field. Observations of oval motion can thus at least set an important upper limit to the size of the dipole tilt of the internal planetary field. Here we report that Saturn's southern auroral oval does indeed oscillate, with an elliptical motion of semimajor axis ∼1–2° in amplitude, and with a period of ∼10.76 h ± 0.15 h. This result places an independent constraint on the magnitude of the planet's dipole tilt and may also indicate the presence of an external current system that imposes an asymmetry in the ionospheric field modulated close to the planetary period.

2. Observations

[5] Saturn's ultraviolet (UV) auroras have been observed for many years [*Broadfoot et al.*, 1981; *Clarke et al.*, 1981; *Gérard et al.*, 1995] but recently high-resolution images using the Hubble Space Telescope (HST) Space Telescope Imaging Spectrograph and Advanced Camera for Surveys (ACS) have revealed highly dynamic auroral emissions that are controlled to a significant degree by the solar wind [*Gérard et al.*, 2004; *Clarke et al.*, 2005; *Grodent et al.*, 2005]. Saturn's auroras generally take the form of a ∼2° wide ring or spiral fixed in local time (i.e., the pattern is independent of the rotation of the planet) whose poleward and equatorward boundaries have median locations of ∼14° and ∼16° colatitude, respectively at noon, although these are highly variable, ranging from 2° to 20° for the former and between 6° and 23° for the latter [*Clarke et al.*, 2005; *Grodent et al.*, 2005; *Badman et al.*, 2006]. Auroral rings can be formed by ionospheric flow shears due to either momentum transfer internal to the magnetosphere, such as the system associated with Jupiter's main auroral oval [*Hill*, 2001; *Cowley and Bunce*, 2001; *Nichols and Cowley*, 2004],

or the solar wind interaction at the open-closed field line boundary [*Cowley et al.*, 2004a]. Theoretical analysis [*Cowley et al.*, 2004b], statistical studies of the location of the auroral emission [*Badman et al.*, 2006], and the recent observation of a field-aligned current at the open-closed field line boundary coincident with HST images of the aurora [*Bunce et al.*, 2008a] indicate that the latter is more likely in Saturn's case. The above mentioned studies have assumed that the spin and magnetic axes are coaligned, such that any change in the auroral oval boundary locations has been associated with the amount of open flux present in the magnetic tail, and no connection of the overall position of the oval with planetary rotation has thus far been made. We address this issue in the present paper.

[6] In January 2007 and February 2008 HST campaigns were undertaken in which Saturn was observed for one HST orbit every day over the intervals 13–26 January in 2007 and 1–16 February in 2008, i.e., over some 29 and 32 Saturn rotations, respectively (J. T. Clarke et al., The response of Jupiter's and Saturn's auroral activity to the solar wind, submitted manuscript, 2008). This extended period of observation, during which a total of 839 exposures were obtained using the Solar-Blind Channel (SBC) of the ACS, has resulted in unprecedented temporal and longitudinal coverage of Saturn's southern UV auroras (only the southern auroras were visible from Earth due to the present $\sim 14^\circ$ tilt of the southern pole toward the Sun). The ACS/SBC instrument consists of a 1024×1024 MultiAnode Microchannel Array detector with an average scale of ~ 0.032 arcsec pixel^{-1}, such that the overall field of view is 35×31 arcsec^2, large enough to encompass Saturn and a significant portion of the rings. Images were taken in groups of five using the F115LP, F125LP, and F140LP longpass filters, which have short wavelength cutoffs of 115 nm, 125 nm, and 140 nm, respectively. The F115LP filter admits H_2 Lyman and Werner bands and H Lyman-α emission, the F125LP filter mostly excludes the H Lyman-α band, and the F140LP filter excludes all the Werner and Lyman-α emission. For further details of the spectra of outer planet auroral emission, see, e.g., *Clarke et al.* [2004] and *Gérard et al.* [2002]. During each 100 s exposure the blurring introduced by planetary rotation of any corotating features is $\sim 1^\circ$ at the central meridian longitude (CML). The raw images were reduced using a custom-built pipeline in which the images were corrected for geometric distortion and scaled to 0.025 arcsec pixel^{-1}, flat-fielded and dark-count calibrated using the latest calibration files available from the Space Telescope Science Institute. The images were then converted from counts pixel^{-1} to kR of H_2 plus Lyman-α emission (where 1 kR represents a photon source flux of 10^9 cm^{-2} s^{-1} radiating into 4π steradians) using the conversion factors 1 kR = 2.103×10^{-3}, 1.473×10^{-3}, and 7.436×10^{-4} counts s^{-1} pixel for the F115LP, F125LP, and F140LP filters, respectively. These conversion factors were calculated using the *Gérard et al.* [2002] synthetic UV spectrum of H_2 plus Lyman-α emission.

[7] The position angle of the planet's spin axis was obtained from the NASA Navigation and Ancillary Information Facility SPICE system [*Acton*, 1996]. The planet center pixel was found by manually fitting simulations of the major rings and the planet's limb (taken to be the height of the homopause, estimated to be 650 km above the 1 bar level at auroral latitudes, taking into account the planet's obliquity and the terminator) as viewed from HST to each group of images. The ring boundaries are useful for this purpose since they are very sharp and independent of planetary surface features and thus should not introduce systematic error at the planetary period. This procedure is estimated to be accurate to within 2 pixels in both vertical and horizontal directions, approximately equal to the point-spread function of the instrument. The movie file Movie S1 in the auxiliary material shows the reduced images with the computed latitude-longitude grid and major ring boundary locations overlaid.[1] The location of the modeled ring boundary locations is consistent with observation in all the images and indicates that the variation of the location of the auroral oval with respect to the spin pole is not an artifact of image reduction. The images obtained are publicly available at http://www.bu.edu/csp/PASS/main.html.

[8] Planetocentric projections were generated from the reduced images, which simulate a viewpoint looking down from above the north pole, i.e., through the planet for the case of the southern auroras, with the central meridian longitude (CML) oriented toward the bottom. This simulated viewpoint is conventional for Earth's auroras since it allows easy comparison with images of the northern auroras and satellite data, where available. We note, however, that the Earth's auroras are generally plotted in magnetic coordinates, whereas here we use kronicentric coordinates referenced to the spin axis. The accuracy of the projection decreases toward the limb of the planet due to the increasing obliquity of the planet's surface with respect to the observer, so the projections are clipped a few degrees from the limb to remove the inaccurate artificially stretched region. We note that the planet's oblateness of 0.09796 is taken into account in the procedure, and for further details of the accuracy of the projections, see *Grodent et al.* [2005]. Groups of five images were superposed in order to increase the signal-to-noise at the cost of longitudinal blurring due to the planet's rotation of up to $\sim 5^\circ$ at the CML for corotating features. This is an upper limit, since the blurring is reduced at longitudes away from the CML and in reality features are observed to slide along the oval at ~ 20–70% of corotation. The auroral emission was further highlighted by the subtraction of a simulated reflected sunlight background disc. The disc was created by fitting modified Minnaert functions [*Vincent et al.*, 2000] separately to the dawn and dusk limbs and then applying a latitudinal intensity profile in which the auroral region intensity was linearly interpolated from lower latitudes. The background was removed such that the residual counts equatorward of the auroral oval, representing experimental noise, sum to zero. An example of an averaged projected image with the background removed is shown in Figure 2.

3. Analysis

3.1. Determination of the Oval Location

[9] The "location" of Saturn's auroral emission, as defined by the poleward and equatorward boundaries, has

[1] Auxiliary materials are available in the HTML. doi:10.1029/2008JA013444.

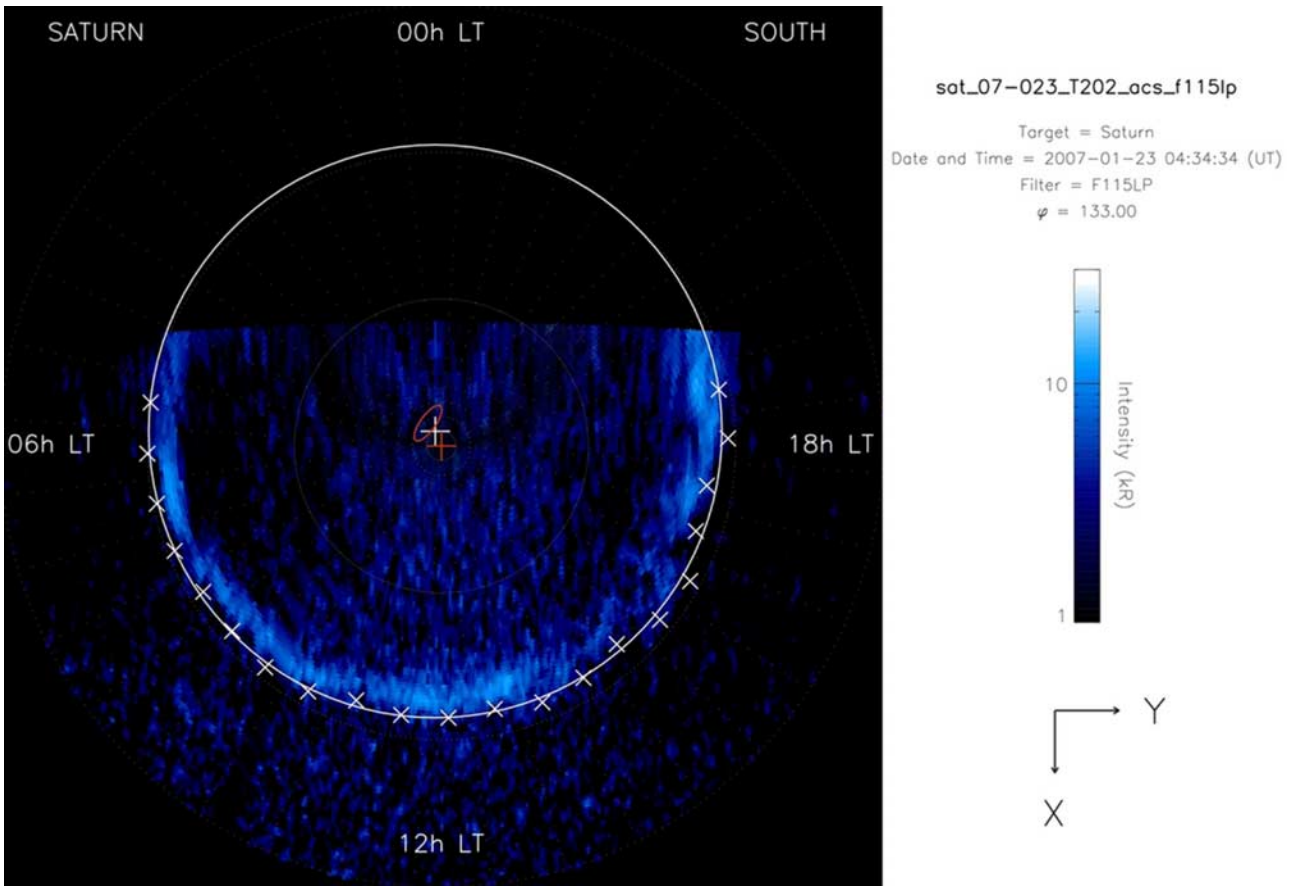

Figure 2. An example of a projected HST/ACS-SBC image of Saturn with the reflected sunlight background removed. The image has been log-stretched and saturated at 30 kR, and a dotted 10° latitude-longitude grid is overlaid. The view is simulated such that the observer is looking from above the north pole and the CML is directed to the bottom of the image, such that dawn is to the left and dusk to the right. The red cross shows the location of the kronographic pole. The white circle shows a fit to the equatorward boundary locations shown by the diagonal crosses and the larger white cross indicates its center. The labeled arrows show the directions of the X and Y axes as defined in the text.

been shown to be highly variable, especially the poleward boundary [*Clarke et al.*, 2005; *Grodent et al.*, 2005; *Badman et al.*, 2006], which under the above physical interpretation may be representative of the open-closed field line boundary. In this study we have modeled the location of the auroral emission with circles fitted to the equatorward boundaries of the auroral emission. We note that this approach differs from studies of the terrestrial auroras [e.g., *Carbary et al.*, 2003], in which Gaussians are fitted to the latitudinal intensity profiles, but we chose the equatorward boundary for a number of reasons. First, the equatorward boundary is more stable and circular than the poleward boundary, which is sometimes modified by poleward expansions that make fitting a circle inappropriate. Indeed, in many cases emission extends high into the polar region and the location of the poleward boundary is very hard to detect, if one exists at all. In addition the aurora is emitted from a ~1000 km high curtain, which is not taken into account in the projection routine. The "poleward" edge of the oval is thus modified by the finite height of the curtain, due to the obliquity of the view from Earth, with varying effect around the oval. The equatorward edge is not affected by the obliquity of the view. The fitting was done with an automated fitting routine which first sums the image over 10° longitude bins to increase the signal to noise, then, for each longitude bin which exhibits a sharp equatorward boundary, measures the latitude of the large negative gradient associated with the decrease in intensity on the equatorward edge of the oval, and finally computes the best fit circle along with associated uncertainties. Only those images that exhibited auroral emission to which a circle could be reasonably fitted were considered, such that images with a distinctly nonoval morphology or those with an auroral arc less than a quarter of circle in length were discarded. The discarded images numbered 14 out of 52 images for 2007 and 26 out of 78 for 2008, and their occurrence is not linked to a specific CML or phase, since Saturn's auroral morphology is determined by conditions in the interplanetary medium [*Clarke et al.*, 2005; Clarke et al., submitted manuscript, 2008]. The mean of the standard errors between the boundary locations and the best fit circles is ~1.04° and ~1.48° for 2007 and 2008, respectively, values which represent ~6% and ~8% of the mean circle radius of 18°. A circle thus represents a reasonable first-

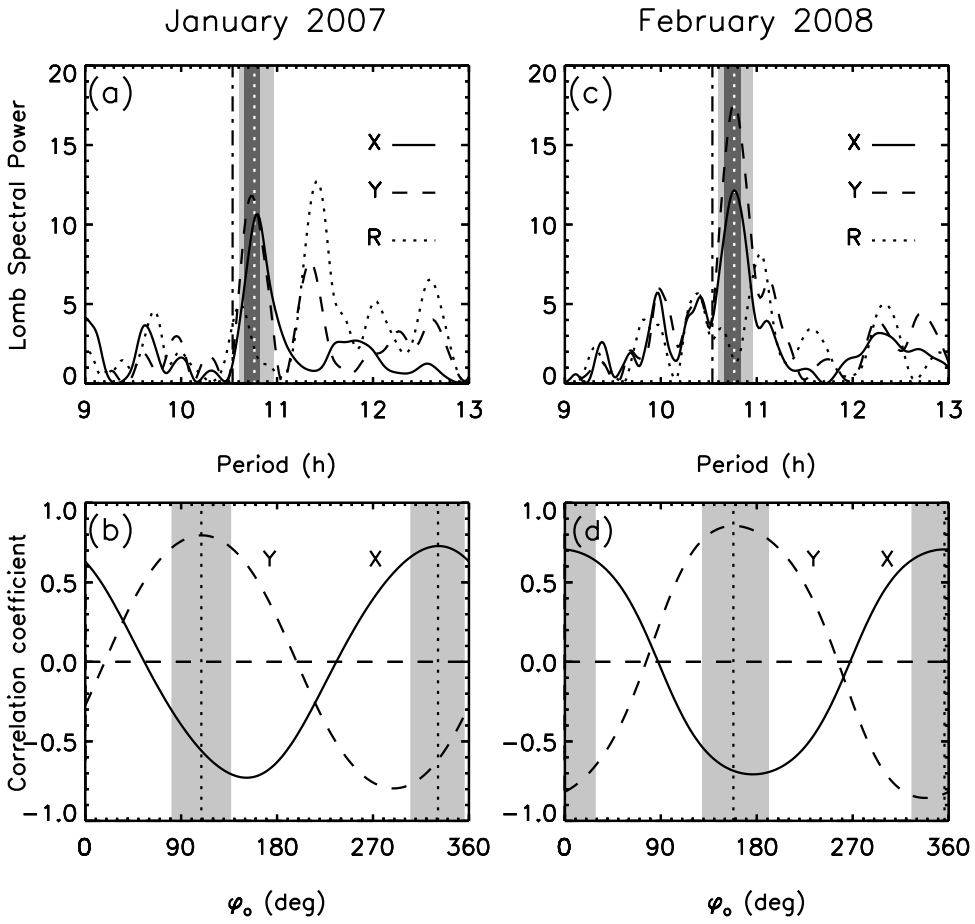

Figure 3. (a and c) Lomb periodograms of spectral power versus period for the X (solid line), Y (dashed line) and R (dotted line) parameters of the fitted circles for 2007 and 2008, respectively. The light gray shaded areas indicate the region between the combined FWHM limits. The dark gray regions are bounded on the left by the IAU period of ~10.66 h [*Desch and Kaiser*, 1981] and on the right by the January 2007 SKR period of 10.82 h (Figure 3a) and February 2008 SKR period of 10.83 h (Figure 3c) [*Kurth et al.*, 2008]. The dot-dashed line at 10.54 h indicates the *Anderson and Schubert* [2007] period. The white dotted lines at 10.75 h (Figure 3a) and 10.79 h (Figure 3c) shows the mean of the two peak locations. (b) and (d) The correlation coefficient between the fitted circle center locations and sin φ, versus $\varphi_\circ$ for 2007 and 2008, respectively. The gray regions indicate the values of $\varphi_\circ$ for which the correlation coefficient is greater than 90% of the maximum values.

order approximation to the equatorward boundary of the auroral emission, with three degrees of freedom: X, Y, and R, where (X,Y) are the coordinates of the circle center in a Cartesian system centered on the spin pole, with unit lengths in both directions corresponding to one degree of colatitude from the pole. The X and Y axes are defined such that X is positive toward HST (differing from the sunward direction by only ~2° since Saturn was near opposition during both campaigns), Y is positive toward dusk, and R is the circle radius. An example of a fitted circle is shown by the white circle with the cross in the center in Figure 2, along with the locations of the detected boundary locations. Movies S2 and S3 in the auxiliary material are movies containing all the projected images and fitted circles obtained in this study, arranged in increasing phase φ determined from the Lomb and correlation analyses described below. The auroral oval in Figure 2 exhibits a displacement toward midnight and dawn, typical of the images taken during this campaign as highlighted by the best fit analysis discussed below. The displacement toward midnight is consistent with previous observations and is presumably due to solar wind pressure on the dayside. The general offset toward dawn is interesting, since the oval has been observed previously to be biased toward the duskside [*Badman et al.*, 2006].

3.2. Oscillation of the Oval

[10] The oscillation period was determined from the circle X and Y position values using a Lomb analysis. This technique is useful for identifying sinusoidal periodicities in irregularly spaced data such as the fitted circle locations determined in this study. Results for 2007 and 2008 are shown in Figures 3a and 3c, respectively, in which Lomb spectral power is plotted versus rotation period for the X (solid line) and Y (dashed line) components and R (dotted line). Colocated peaks in the X and Y periodograms are evident in both 2007 and 2008 periodograms. Numerical values of the peak locations, heights, significance, signal-to-

Table 1. Parameters of the Oscillation of the Auroral Oval

		2007		2008	
Analysis	Parameter	X	Y	X	Y
Lomb analysis peak	Peak Lomb spectral power	10.33	11.54	12.15	17.61
	Significance level	6.3×10^{-3}	1.9×10^{-3}	1.4×10^{-3}	5.7×10^{-6}
	Signal-to-noise ratio	3.1	5.0	3.5	5.9
	Peak period τ (h)	10.80	10.73	10.76	10.76
	FWHM (h)	0.30	0.30	0.34	0.36
Cross-correlation analysis	Correlation coefficient maximum value	0.73	0.80	0.71	0.86
	Phase $\varphi_\circ$ at maximum correlation value (°)	331	110	356	158
	Width of 90% of max correlation region (°)	51	56	64	62
Linear regression	Gradient (= α, β) (°)	1.2	0.9	1.8	1.3
	Intercept (= x_o, y_o) (°)	−1.5	−0.9	−1.7	−1.4
	Standard error between fit and data	0.80	0.53	1.4	0.61
	Standard error of regression gradient	0.19	0.11	0.25	0.11
Lissajous ellipse	Semimajor axis (°)	1.4		2.2	
	Semiminor axis (°)	0.5		0.3	
	Eccentricity	0.93		0.99	
	Orientation (°)	54		54	

noise ratio, and width are given in Table 1. The mean location of the X and Y peaks is 10.76 h for 2007, while for 2008 the both peaks are located at 10.76 h, values shown in Figures 3a and 3c by the white dotted vertical lines. Also shown in the figure are quantitative estimates of the significance of the peaks in the periodograms [*Press et al.*, 2007]. A peak should only be considered significant if the significance level is $\ll 1$, a condition that is well satisfied by the significance levels for the X and Y peaks. The signal-to-noise ratios of the peaks are ~3–6, with the Y peak having higher values in both cases. The full-width at half-maximum (FWHM) values for these peaks, as indicated by the light-gray regions in Figures 3a and 3c, are all ~0.3 h, indicating an uncertainty in the determination of the oscillation period of ±~0.15 h. The uncertainty in the period is related to the error in the determination of the oscillation phase by $\Delta\tau = (\tau^2/T)(\Delta\varphi/360)$, where T is the length of time over which measurements are made and $\Delta\varphi$ is the uncertainty in the oscillation phase determination. Employing a time period of 13 days to make measurements with which the phase can be determined to roughly a quarter of a cycle (see below) implies an uncertainty in the estimation of the period of ~0.1 h, similar to the FWHM of the peaks in the Lomb periodograms. The dark gray regions, bound on the left by the Voyager-era IAU period of ~10.66 h and on the right by the respective SKR/FGM periods of 10.82 h for January 2007 and 10.83 h February 2008, indicates the range of periods associated with the SKR emission. Also shown for comparison is the period derived by *Anderson and Schubert* [2007] (dot-dashed line at 10.54 h). The mean peak period of 10.76 h is thus consistent with the SKR and magnetometer values within the FWHM of the peaks and slightly longer than that derived from gravitational data.

[11] Considering now the R periodogram, there are no significant peaks colocated with those for X and Y, indicating that the variation in circle location is not due to changes in the size of the observed section of the oval. A peak is evident at ~11.4 h for 2007; however, recent evidence suggests that the open-closed field line boundary may be associated with the poleward edge of the auroral oval [*Belenkaya et al.*, 2007; *Bunce et al.*, 2008a], such that this boundary may be expected to exhibit changes as the amount of open flux in the system varies. Since we fit to the equatorward edge of the oval, we would hesitate to infer physical significance from the variation of this parameter, other than it may be indirectly related to the amount of open flux if the width of the auroral emission region is constant (which it is not). The variation of the location of the poleward boundary is an interesting topic; however, it is beyond the scope of this paper and will be studied in future works.

[12] The overall nature of the motion of the oval is determined by the relative phases and amplitudes of the oscillations in the X and Y components. Given that for both 2007 and 2008 the oscillation periods τ determined above are essentially identical for the two components, the overall motion is that of a Lissajous ellipse, whose components are given parametrically by

$$X = x_\circ + \alpha \sin(\varphi_x), \tag{1a}$$

and

$$Y = y_\circ + \beta \sin\left(\varphi_y\right), \tag{1b}$$

where α and β are the amplitudes of the oscillations about centers $x_\circ$ and $y_\circ$, and the phases φ_x and φ_y are given by

$$\varphi_x = (360t/\tau) - \varphi_{x\circ}, \tag{2a}$$

and

$$\varphi_y = (360t/\tau) - \varphi_{y\circ}. \tag{2b}$$

The resulting ellipse has eccentricity ε, given by

$$\varepsilon = \sqrt{1 - \frac{b^2}{a^2}}, \tag{3}$$

where a and b are the semimajor and semiminor axes, respectively, given by

$$a = \frac{\sqrt{2}}{2}\sqrt{\alpha^2 + \beta^2 + \left(\alpha^2 - \beta^2\right)\sqrt{1 + \frac{4\alpha^2\beta^2\cos^2\delta}{\left(\beta^2 - \alpha^2\right)^2}}}, \tag{4}$$

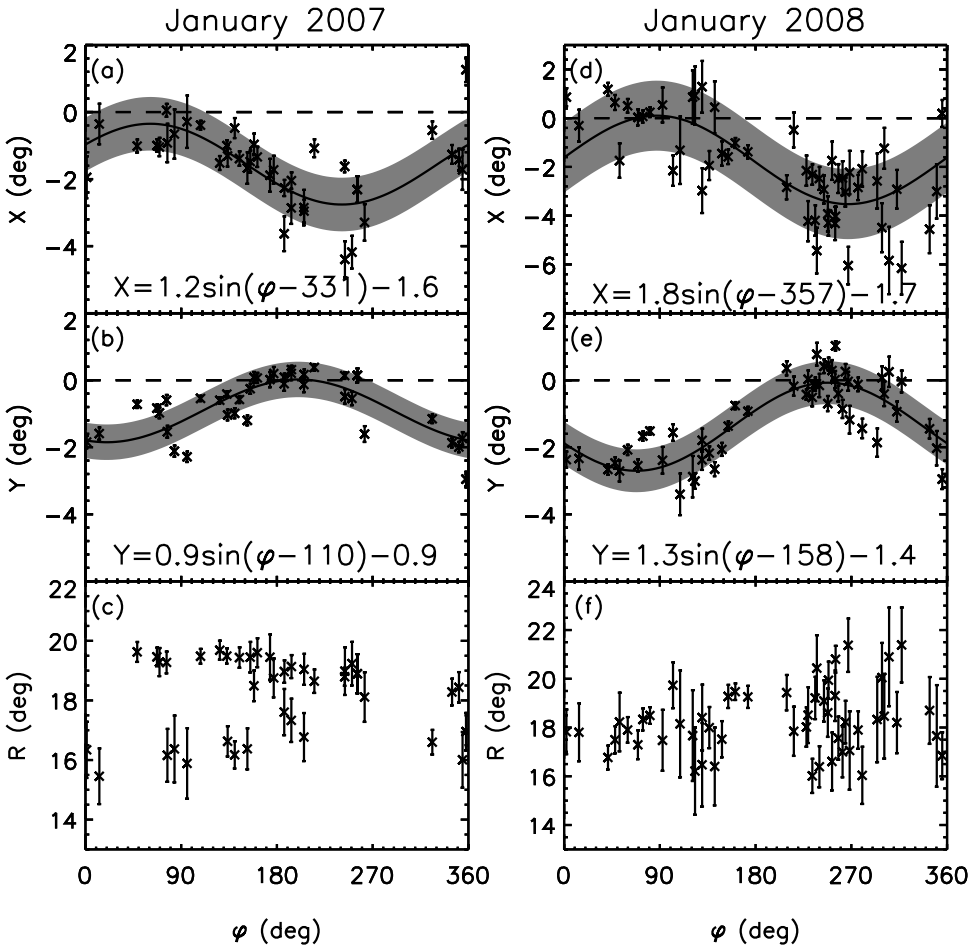

Figure 4. Plots of the parameters of the fitted circles versus phase φ showing (a–c) the results for 2007 and (d–f) the results for 2008. Shown are X (Figures 4a and 4d), Y (Figures 4b and 4e), and R (Figures 4c and 4f), as defined in the text. Note the slightly expanded vertical scale in Figure 4d. The crosses show the values for each summed image, and the error bars indicate the standard errors in the best fit circle parameters. The solid lines indicate the best fit sinusoids to the data using appropriate period and phase values given in Table 1, and the surrounding gray shaded regions represent the standard errors of the data with respect to the fits.

and

$$b = \frac{\sqrt{2}}{2}\sqrt{\alpha^2 + \beta^2 - \left(\alpha^2 - \beta^2\right)\sqrt{1 + \frac{4\alpha^2\beta^2\cos^2\delta}{\left(\beta^2 - \alpha^2\right)^2}}}, \quad (5)$$

where $\delta = \varphi_{x\circ} - \varphi_{y\circ}$ is the difference between the phases of the X and Y component oscillations. The orientation ϕ of the ellipse measured relative to the dawn-dusk line is given by

$$\phi = \frac{1}{2}\tan^{-1}\left(\frac{2\alpha\beta\cos\delta}{\alpha^2 - \beta^2}\right). \quad (6)$$

The parameters $\varphi_{x\circ}$ and $\varphi_{y\circ}$ are determined below, followed by α and β.

[13] Taking the above mean period of τ = 10.76 h for both 2007 and 2008, respectively, the phases of the oscillations were determined using a cross-correlation analysis between the circle center X and Y positions and the sine of phase φ, given by equation (2), with $\varphi_\circ$ incremented in 1° steps. For simplicity we have taken the zeroes of time t to be at 0000 UT on 1 January 2007 and 2008, respectively. The correlation coefficient profiles for X (solid line) and Y (dashed line) are shown versus $\varphi_\circ$ in Figures 3b and 3d. The phase $\varphi_\circ$ with maximum correlation values, along with the values of the cross-correlation coefficient and the width of the region in which the correlation coefficient is greater than 90% of the maximum are given in Table 1. The values of the correlation coefficients are ~0.7–0.9. For 2007 we obtain a phase difference δ of 139°, while for 2008 we have a difference of 162°. The gray boxes in Figures 3b and 3d indicate the values of $\varphi_\circ$ for which the correlation coefficient is greater than 90% of the maximum values, thus indicating the reasonable uncertainty range of the phase determination. The widths of these regions are detailed in Table 1, and the root-sum-square estimates of the uncertainty in δ are ~75° for 2007 and ~87° for 2008.

[14] In Figure 4 we plot the X, Y, and R data versus φ given by equation (2), modulo 360°, with τ and $\varphi_\circ$ taken to

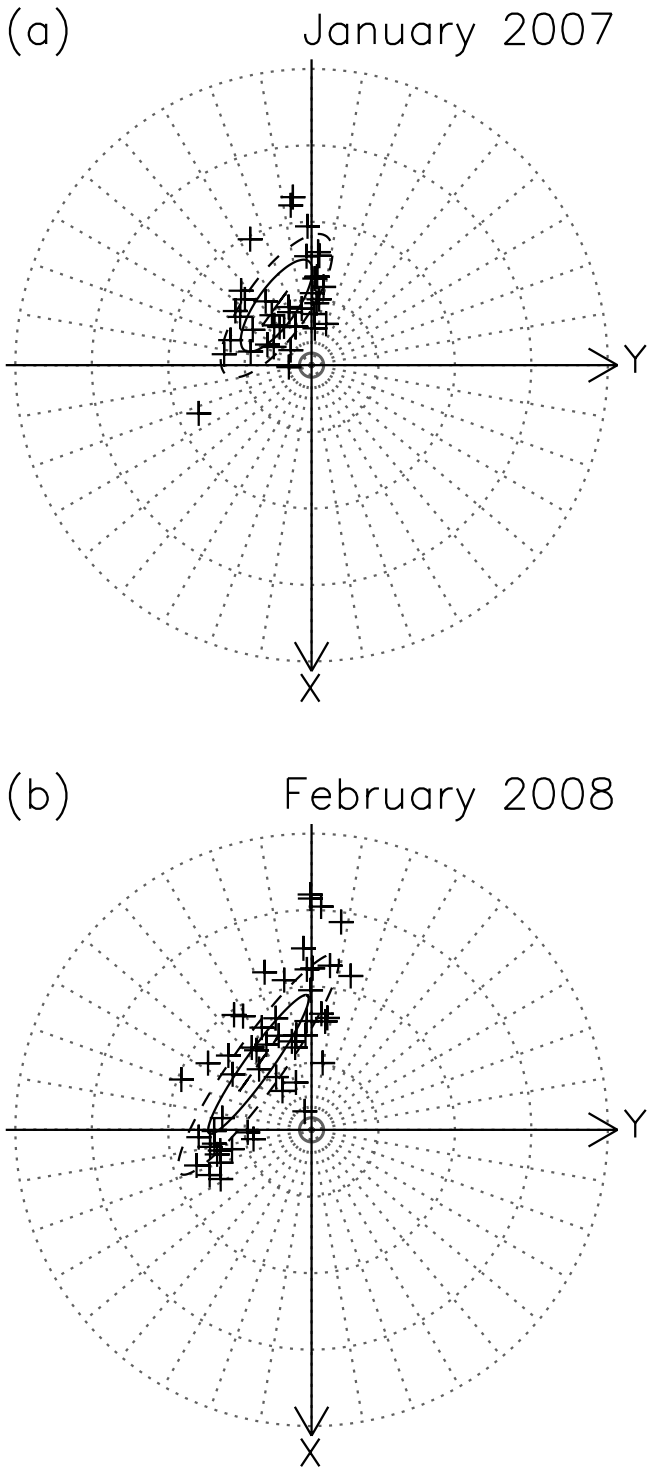

Figure 5. Plots showing the best fit ellipses (solid lines) for (a) 2007 and (b) 2008, along with uncertainty ranges of the axis lengths (dashed lines) and the individual center locations. A 2° latitude × 10° longitude grid is overlaid.

be the appropriate values given in Table 1, determined from the above Lomb and cross-correlation analyses. The error bars show the standard errors of the circle parameters as determined by the best fit routine. The mean of the standard errors in the X component is 0.37° and 0.68° for 2007 and 2008, respectively, while those for the Y component are 0.16° and 0.27°. This difference in the uncertainties between the components arises since the Y component is constrained on both the dawn and dusk sides, while the X component is only constrained on the noonside. Fitting sinusoids to the X and Y data using linear regression yields the oscillation amplitudes α and β, and centers $x_\circ$ and $y_\circ$, values of which are given in Table 1 and shown in Figure 4, along with appropriate uncertainty values. Employing these values in equations (3–6), we obtain ellipse semimajor axis, semiminor axis, eccentricity, and orientation values as tabulated in Table 1. The 2007 data are consistent with the motion of the oval center on an ellipse with semimajor axis ∼1.4° ± 0.3°, and semiminor axis ∼0.5° ± 0.8° (i.e., not well constrained by these data) oriented toward ∼09–21 h ± 0.8 h LT, and offset from the spin axis by ∼1.8° toward ∼04 h LT. Similarly, the 2008 data are consistent with the motion of the oval center about an ellipse with semimajor axis ∼2.2° ± 0.3°, semiminor axis ∼0.3° ± 1.2° (again, not well constrained) oriented toward ∼09–21 h ± 0.5 h LT, and offset from the spin axis by ∼2.2° toward ∼03 h LT. The above uncertainties in the ellipse properties were computed by combining the individual contributing errors in the standard way.

[15] These ellipses are shown in Figure 5 along with the individually determined center locations and also in the Movies S2 and S3 in the auxiliary material for 2007 and 2008, respectively. The best fit ellipses are shown by the solid lines, and the dashed lines show the above uncertainty ranges in the axes. As discussed above, although the ellipse eccentricity is not well constrained in either case, the motion is in each case described by a very eccentric ellipse whose major axis is oriented toward prenoon/premidnight. It is interesting to note here that the SKR has been shown to be emitted predominantly from the morning sector [*Warwick et al.*, 1981; *Lecacheux and Genova*, 1983; *Galopeau et al.*, 1995; *Lamy et al.*, 2008], but the relation of the SKR modulation to the oscillation discussed here remains to be determined. The apparent change of ellipse shape between 2007 and 2008 may be due to either a true phase slippage in the X or Y components relative to each other over this time or the motion is actually similar in both cases and the difference is due to the scatter in the position data. This is presumably due to external, e.g., solar wind-driven, processes modulating the location of the oval, which have not been considered in this work and will be the subject of future studies.

[16] The question remains as to the consistency of the oscillation over timescales longer than a year. The SKR period is variable, but the variation is less than the FWHM of the peaks shown in Figure 3. Data from previous HST campaigns exist from January 2004 and October 2005, upon which the analysis described above has similarly been used to determine the oval locations. The former campaign, however, was specifically designed to concentrate observations over a small CML range and was characterized by large solar wind disturbances and departures from an oval morphology, rendering many of the images unusable in this analysis. The latter campaign only covered five days and in many of the images the auroral emission was too faint to obtain a robust fit. The Lomb periodograms, in the same format as for Figure 3a, are shown in Figure 6. Figure 6a shows the January 2007 result, i.e., that shown in Figure 3a,

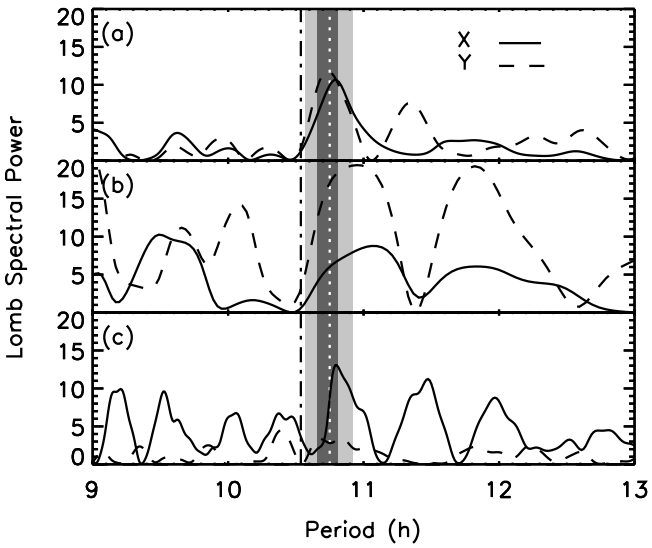

Figure 6. Lomb periodograms, in the same format as for Figures 3a and 3c. (a) The January 2007 result, i.e., that shown in Figure 3a. For comparison, (b) the October 2005 result and (c) the January 2004 result are also shown.

Figure 6b shows the October 2005 result, and Figure 6c shows the January 2004 result. It can be seen that there is no well-defined peak that stands above the noise in the October 2005 trace, probably due to the limitations described above. For January 2004 there is a peak in the X component at 10.80 h but not one for the Y component. This value is consistent with the 10.76 h ± 0.15 h result obtained from the January 2007 and February 2008 data and indicates that the oscillation could be a long-lived phenomenon, although it is impossible to say whether the difference in the periods is real or due to the significant scatter in the data. A statistically significant shift of the rotation period would imply that the rotation is modulated by external processes, e.g., [*Dessler et al.*, 1981; *Hill et al.*, 1981; *Gurnett et al.*, 2007; *Goldreich and Farmer*, 2007], rather than indicating the rotation of the internal field. It will be illuminating to conduct this analysis using future data to investigate the longevity of the oscillation discussed above and also to determine whether the northern oval similarly oscillates.

3.3. Nonaxisymmetric Corotating Convection

[17] To illustrate the effect external currents could have upon the position of the auroral oval, we present the following simple example. *Bunce et al.* [2008a] observed a sheet of upward field-aligned current colocated with the open-closed field line boundary while crossing field lines which map to the auroral oval, and recent work (D. L. Talboys, Characterisation of auroral current systems in Saturn's magnetosphere: High-latitude Cassini observations, manuscript in preparation, 2008) consistently places in situ observations of the field-aligned current within an outer magnetosphere plasma sheet region beyond the main ring current region. According to the model of *Bunce et al.* [2008b] typical auroral colatitudes of ∼15° map, depending on the magnetopause subsolar standoff distance, to 13–26 R_S, i.e., a few R_S inside the magnetopause. We therefore assume that the auroral oval is formed at equatorial distance ∼20 R_S, a value chosen as being representative of this range, and investigate the effect of a nonaxisymmetric current system on the location of the boundary.

[18] At large distances, a current loop centered on and oriented at an angle to the planetary dipole would exactly mimic a tilt in the dipole field. In the present case, the auroral field lines are not very distant from the inferred current loop (see below) and so we find the perturbations numerically. An axisymmetric internal dipole field and ring current (0.4 MA at 15 R_S) are chosen such that unperturbed L = 20 field lines intersect the planet at ∼15° colatitude, a typical observed radius of the auroral oval. The nonaxisymmetric currents are based on the model of *Goldreich and Farmer* [2007] in which these currents feed a system of plasma convection in the magnetosphere. We choose to include the dominant currents only, which are of size 0.4 MA and flow along field lines L = 12, connecting the outer part of the plasma outflow to the ionosphere. This part of the narrow *Goldreich and Farmer* [2007] "tongue" is significantly bent away from radial; for definiteness we place outward and return currents separated by 180° in longitude. The results will be qualitatively similar for any reasonably large angle of separation, and the chosen current distribution may also be compatible with other models of magnetospheric convection. We connect outward and return currents in the equatorial plane at 12 R_S and around the polar cap of the planet. All currents are shown as arrowed blue lines in Figure 7. In the inner magnetosphere, these currents give rise to a nonaxisymmetric azimuthal magnetic field of peak to peak amplitude ∼10 nT, consistent with Cassini measurements [e.g., *Cowley et al.*, 2006]. With the current distribution in place, we integrate from 12 points of equal total field strength in the equatorial plane (B = 4.3 nT, R ∼ 20 Rs) back to the surface of the planet, using the computer program BiotSavart (Ripplon Software). The resulting points of intersection, plotted in Figure 8, are systematically offset toward the current by around 1.5°. Given the various factors neglected in this analysis (obliquity of rotation axis, magnetopause currents, etc.) it is difficult to predict the precise nature of the motion of the oval, but an effect of order 1.5° which varies on the rotation period of the current system is expected on the basis of this model.

4. Summary

[19] In this paper we have examined HST images of Saturn's UV auroras taken over 13 days in January 2007 and 15 days in February 2008, and fitted circles to the equatorward edge of the auroral emission to find the central location of the emission. We have found that the location of the center of the auroral oval oscillates with period 10.76 h ± 0.15 h for both January 2007 and February 2008, i.e., close to the periods determined for oscillations in other magnetospheric phenomena, such as the SKR and magnetic field data. The oscillation is described for 2007 by an ellipse with semimajor axis ∼1.4° ± 0.3°, and semiminor axis ∼0.5° ± 0.8° oriented toward ∼09–21 h ± 0.8 h LT, and offset from the spin axis by ∼1.8° toward ∼04 h LT. For 2008 the oscillation is consistent with an ellipse with semimajor axis ∼2.2° ± 0.3°, semiminor axis ∼0.3° ± 1.2° oriented toward ∼09–21 h ± 0.5 h LT, and offset from the spin axis by ∼2.2° toward ∼03 h LT. Thus, although the eccentricity of

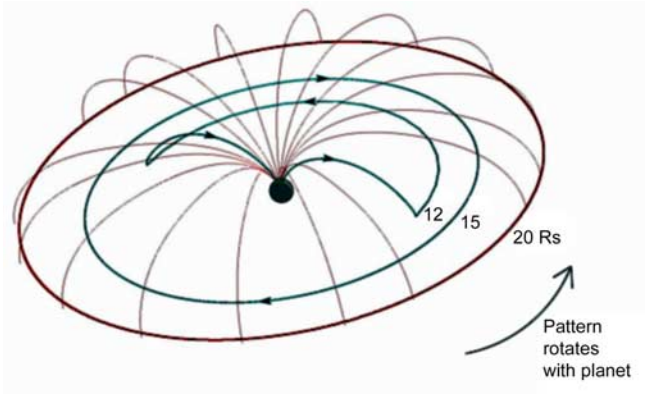

Figure 7. Illustration of the currents and magnetic field used to model the shift of the auroral oval using the theory of *Goldreich and Farmer* [2007]. Currents are shown in blue, magnetic field lines are shown in pink, and a circle of radius 20 R_S, taken to represent the source location of the auroras as being near the open-closed field line boundary, is shown in red.

the ellipses is not well constrained in either case, the motion appears very elliptical for both 2007 and 2008, and in each case the major oscillation axis is oriented toward prenoon/premidnight.

[20] This oscillation of the oval is a previously unknown phenomenon. Importantly, it is observed in the polar ionosphere, where at ~50,000 nT the internal field is dominant, rather than in the more distant magnetosphere where the field is much weaker and more susceptible to modulation by external processes. Given the uncertainty in the nature of the motion, it is not possible to say precisely what the cause of the oscillation is. If the motion were obviously circular, the simplest explanation would be that it represents the motion of the magnetic pole as a ~1° tilted dipole rotates with the period of the deep planetary interior. The counterintuitive result that the kronographic pole lies outside the radius of rotation would then occur because the solar wind offset is comparable to the magnitude of the dipole tilt, and the overall location is the sum of these effects. Only if the dipole tilt were greater than the offset due to the solar wind, e.g., as at Earth, would the kronographic pole lie within the radius of rotation. This explanation would, however, raise questions as to why the oscillation appears to be elliptical, or even linear from morning to evening, rather than circular as would be expected from a dipole tilt; why this period is longer than that derived from gravitational data by *Anderson and Schubert* [2007]; and also why a ~1° dipole tilt has not been definitively observed in near-planetary magnetometer data.

[21] Thus, while we cannot entirely rule out an internal source for the oscillation, given that the motion appears to be elliptical, there is probably some other external process that contributes to the oscillation. Importantly, this observation provides the first constraint of the tilt of Saturn's dipole that is not inferred from magnetometer data and is consistent with the canonical upper limit of the latter. A second possible explanation mentioned above is that the oscillation of the auroral oval is caused by a magnetospheric current system, such as that due to nonaxisymmetric magnetospheric convection [*Dessler et al.*, 1981; *Hill et al.*, 1981; *Gurnett et al.*, 2007; *Goldreich and Farmer*, 2007], which reproduces the effect of a tilted dipole, and we have shown how the current system envisaged by *Goldreich and Farmer* [2007] may lead to a ~1° shift of the auroral oval. Recently, *Southwood and Kivelson* [2007] discussed on the basis of Cassini magnetometer observations a magnetospheric current system flowing on field lines threading the equatorial plane around 11–15 R_S, which would mimic a tilted dipole of 12–18° beyond this distance. Such a tilt is clearly much larger than that discussed here, but the effect may be reduced considerably in the ionosphere [*Kivelson and Southwood*, 2007]. In either case, a naïve application of such rotating current system would also lead to a circular, rather than elliptical, motion of the auroral oval, such that further work on the relation of such rotating current systems to the motion of the auroral oval is clearly warranted.

[22] In addition, an HST campaign is scheduled to observe Saturn near its equinox in 2009, providing the optimum viewing geometry required to observe both poles simultaneously to determine whether the north and south ovals oscillate in phase or antiphase and also determine whether the overall location and morphology of the northern auroras are similar to the south. Although the view will be highly oblique, the dawn-dusk motion at least should be detectable since it is less dependent on the obliquity of the view than the noon-midnight motion. If it turns out that the conjugate auroral ovals oscillate in antiphase then the cause is likely to be a tilted dipole or an external current system which produces similar antisymmetric displacements associated

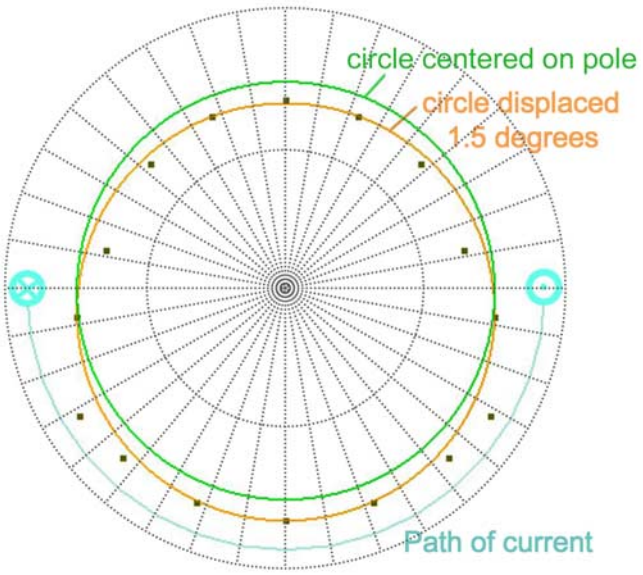

Figure 8. Plot showing the result in the ionosphere of the numerical integration using the model of *Goldreich and Farmer* [2007]. A 15° radius circle centered on the pole is shown in light green, the ionospheric mapping of 12 points of equal field strength in the equatorial plane are shown in dark green, the ionospheric path of the model current is shown in blue and a circle displaced 1.5° toward the current, illustrative of the overall displacement of the twelve points, is shown in yellow. A 10° × 10° latitude-longitude grid is overlaid.

with azimuthal field perturbations that are symmetric about the equator. If, on the other hand, they oscillate in phase then an external current system that produces displacements symmetric about the equator, i.e., associated with antisymmetric azimuthal field perturbations, is probably the source. Interestingly, at all times other than equinox the model of *Goldreich and Farmer* [2007], predicts an asymmetric north–south response. At equinox, they predict that the magnetic perturbations from the north and south hemispheres will be opposite, thus the displacement will be symmetric in the north and south. Until we obtain simultaneous conjugate auroral oval images with HST the north–south symmetry will remain an ambiguity of the result. With regard to the rotation period, under the interpretation that the oval rotation is due to an external current system, then the period may vary over time, as does the period of the SKR. If, despite the ellipticity of the motion, the oscillation is due to an internal source, then this work may represent an observation of the rotation of Saturn's deep interior, albeit with a somewhat low frequency resolution, with a period of $\sim$10.75 h $\pm$ 0.15 h, the lower of the two values obtained here. The uncertainties in the period encompasses the range of rotation periods previously measured from the SKR and magnetometer data, mainly due to the limited volume of HST data currently available compared to the near-continuous Cassini data obtained since orbit insertion in 2004. However, the accuracy to which the period can be determined using this method is dependent on the length of time over which observations can be made, and since the measurements were taken using an Earth-based platform they are not dependent on the longevity of the Cassini mission.

[23] **Acknowledgments.** This work is based on observations made with the NASA/ESA Hubble Space Telescope, obtained at the Space Telescope Science Institute, which is operated by AURA, Inc. for NASA. Work at Boston was supported during the course of this study by NASA grant HST-GO-10862.01-A from the Space Telescope Science Institute to Boston University. JCG and DG are supported by the Belgian Fund for Scientific Research (FNRS) and the PRODEX Programme managed by the European Space Agency in collaboration with the Belgian Federal Science Policy Office. SWHC was supported by STFC grant PP/D002117/1 and a Royal Society Leverhulme Trust Senior Research Fellowship. JDN wishes to thank Alex Dessler, Wayne Pryor, Emma Bunce, and Steve Milan for illuminating discussions regarding the oval rotation.

[24] Wolfgang Baumjohann thanks James F. Carbary and Donald Mitchell for their assistance in evaluating this paper.

References

Acton, C. H. (1996), Ancillary data services of NASA's Navigation and Ancillary Information Facility, *Planet. Space Sci.*, *44*(1), 65–70, doi:10.1016/0032-0633(95)00107-7.

Anderson, J. D., and D. Schubert (2007), Saturn's gravitational field, internal rotation, and interior structure, *Science*, *317*, 1384–1387, doi:10.1126/science.1144835.

Badman, S. V., S. W. H. Cowley, J.-C. Gérard, and D. Grodent (2006), A statistical analysis of the location and width of Saturn's southern auroras, *Ann. Geophys.*, *24*, 3533–3545.

Belenkaya, E. S., I. I. Alexeev, M. S. Blokhina, S. W. H. Cowley, S. V. Badman, V. V. Kalegaev, and M. S. Grigoryan (2007), IMF dependence of the open-closed ?eld line boundary in Saturn's ionosphere, and its relation to the UV auroral oval observed by the Hubble Space Telescope, *Ann. Geophys.*, *25*, 1215–1226.

Broadfoot, A. L., et al. (1981), Extreme ultraviolet observations from Voyager 1 encounter with Saturn, *Science*, *212*, 206–211, doi:10.1126/science.212.4491.206.

Bunce, E. J., et al. (2008a), Origin of Saturn's aurora: Simultaneous observations by Cassini and the Hubble Space Telescope, *J. Geophys. Res.*, *113*, A09209, doi:10.1029/2008JA013257.

Bunce, E. J., C. S. Arridge, S. W. H. Cowley, and M. K. Dougherty (2008b), Magnetic field structure of Saturn's dayside magnetosphere and its mapping to the ionosphere: Results from ring current modeling, *J. Geophys. Res.*, *113*, A02207, doi:10.1029/2007JA012538.

Carbary, J. F., T. Sotirelis, P. T. Newell, and C.-I. Meng (2003), Auroral boundary correlations between UVI and DMSP, *J. Geophys. Res.*, *108*(A1), 1018, doi:10.1029/2002JA009378.

Carbary, J. F., D. G. Mitchell, S. M. Krimigis, and N. Krupp (2007a), Electron periodicities in Saturn's outer magnetosphere, *J. Geophys. Res.*, *112*, A03206, doi:10.1029/2006JA012077.

Carbary, J. F., D. G. Mitchell, S. M. Krimigis, D. C. Hamilton, and N. Krupp (2007b), Charged particle periodicities in Saturn's outer magnetosphere, *J. Geophys. Res.*, *112*, A06246, doi:10.1029/2007JA012351.

Carbary, J. F., D. G. Mitchell, S. M. Krimigis, and N. Krupp (2007c), Evidence for spiral pattern in Saturn's magnetosphere using the new SKR longitudes, *Geophys. Res. Lett.*, *34*, L13105, doi:10.1029/2007GL030167.

Clarke, J. T., H. W. Moos, S. K. Atreya, and A. L. Lane (1981), IUE detection of bursts of H Ly α emission from Saturn, *Nature*, *290*, 226–227, doi:10.1038/290226a0.

Clarke, J. T., D. Grodent, S. W. H. Cowley, E. J. Bunce, P. Zarka, J. E. P. Connerney, and T. Satoh (2004), Jupiter's auroras, in *Jupiter: The Planet, Satellites and Magnetosphere*, edited by F. Bagenal, T. E. Dowling, and W. B. McKinnon, pp. 639–670, Cambridge Univ. Press, Cambridge, U.K.

Clarke, J. T., et al. (2005), Morphological differences between Saturn's ultraviolet aurorae and those of the Earth and Jupiter, *Nature*, *433*, 717–719, doi:10.1038/nature03331.

Clarke, K. E., et al. (2006), Cassini observations of planetary-period oscillations of Saturn's magnetopause, *Geophys. Res. Lett.*, *33*, L23104, doi:10.1029/2006GL027821.

Cowley, S. W. H., and E. J. Bunce (2001), Origin of the main auroral oval in Jupiter's coupled magnetosphere-ionosphere system, *Planet. Space Sci.*, *49*, 1067–1088, doi:10.1016/S0032-0633(00)00167-7.

Cowley, S. W. H., E. J. Bunce, and R. Prangé (2004a), Saturn's polar ionospheric flows and their relation to the main auroral oval, *Ann. Geophys.*, *22*, 1379–1394.

Cowley, S. W. H., E. J. Bunce, and J. M. O'Rourke (2004b), A simple quantitative model of plasma flows and currents in Saturn's polar ionosphere, *J. Geophys. Res.*, *109*, A05212, doi:10.1029/2003JA010375.

Cowley, S. W. H., D. M. Wright, E. J. Bunce, A. C. Carter, M. K. Dougherty, G. Giampieri, J. D. Nichols, and T. R. Robinson (2006), Cassini observations of planetary-period magnetic field oscillations in Saturn's magnetosphere: Doppler shifts and phase motion, *Geophys. Res. Lett.*, *33*, L07104, doi:10.1029/2005GL025522.

Desch, M. D., and M. L. Kaiser (1981), Voyager measurement of the rotation period of Saturn's magnetic field, *Geophys. Res. Lett.*, *8*(3), 253–256, doi:10.1029/GL008i003p00253.

Dessler, A. J., R. R. Sandel, and S. K. Atreya (1981), The Jovian hydrogen bulge: Evidence for co-rotating magnetospheric convection, *Planet. Space Sci.*, *29*, 215–224, doi:10.1016/0032-0633(81)90035-0.

Dougherty, M. K., et al. (2005), Cassini magnetometer observations during Saturn orbit insertion, *Science*, *307*, 1266–1270, doi:10.1126/science.1106098.

Espinosa, S. A., and M. K. Dougherty (2000), Periodic perturbations in Saturn's magnetic field, *Geophys. Res. Lett.*, *27*, 2785–2788, doi:10.1029/2000GL000048.

Galopeau, P. H. M., and A. Lecacheux (2000), Variations of Saturn's radio rotation period measured at kilometer wavelengths, *J. Geophys. Res.*, *105*, 13,089–13,101, doi:10.1029/1999JA005089.

Galopeau, P. H. M., P. Zarka, and D. Le Quéau (1995), Source location of Saturn's kilometric radiation: The Kelvin-Helmholtz instability hypothesis, *J. Geophys. Res.*, *100*, 26,397–26,410, doi:10.1029/95JE02132.

Gérard, J.-C., V. Dols, D. Grodent, J. H. Waite, G. R. Gladstone, and R. Prangé (1995), Simultaneous of the Saturnian aurora and polar haze with the HST/FOC, *Geophys. Res. Lett.*, *22*, 2685, doi:10.1029/95GL02645.

Gérard, J.-C., J. Gustin, and D. Grodent (2002), Excitation of the FUV Io tail on Jupiter: Characterization of the electron precipitation, *J. Geophys. Res.*, *107*(A11), 1394, doi:10.1029/2002JA009410.

Gérard, J.-C., D. Grodent, J. Gustin, A. Saglam, J. T. Clarke, and J. T. Trauger (2004), Characteristics of Saturn's FUV aurora observed with the Space Telescope Imaging Spectrograph, *J. Geophys. Res.*, *109*, A09207, doi:10.1029/2004JA010513.

Giampieri, G., M. K. Dougherty, E. J. Smith, and C. T. Russell (2006), A regular period for Saturn's magnetic field that may track its internal rotation, *Nature*, *441*, 62–64, doi:10.1038/nature04750.

Goldreich, P., and A. J. Farmer (2007), Spontaneous axisymmetry breaking of the external magnetic field at Saturn, *J. Geophys. Res.*, *112*, A05225, doi:10.1029/2006JA012163.

Grodent, D., J. T. Clarke, J. Kim, J. H. Waite Jr., and S. W. H. Cowley (2003), Jupiter's main oval observed with HST-STIS, *J. Geophys. Res.*, *108*(A11), 1389, doi:10.1029/2003JA009921.

Grodent, D., J.-C. Gérard, S. W. H. Cowley, E. J. Bunce, and J. T. Clarke (2005), Variable morphology of Saturn's southern ultraviolet aurora, *J. Geophys. Res.*, *110*, A07215, doi:10.1029/2004JA010983.

Gurnett, D. A., et al. (2005), Radio and plasma wave observations at Saturn from Cassini's approach and first orbit, *Science*, *307*, 1255–1259, doi:10.1126/science.1105356.

Gurnett, D. A., A. M. Persoon, W. S. Kurth, J. B. Groene, T. F. Averkamp, M. K. Dougherty, and D. J. Southwood (2007), The variable rotation period of the inner region of Saturn's plasma disk, *Science*, *316*, 442–445, doi:10.1126/science.1138562.

Hill, T. W. (2001), The jovian auroral oval, *J. Geophys. Res.*, *106*, 8101–8108, doi:10.1029/2000JA000302.

Hill, T. W., A. J. Dessler, and L. J. Maher (1981), Corotating magnetospheric convection, *J. Geophys. Res.*, *86*(A11), 9020–9028, doi:10.1029/JA086iA11p09020.

Khurana, K. K., C. S. Arridge, M. K. Dougherty, and C. T. Russell (2007), Field periodicities caused by a tilted rotating current sheet in Saturn's magnetosphere, paper presented at the Magnetospheres of the Outer Planets conference, Southwest Res. Inst., San Antonio, Tex.

Kivelson, M. G., and D. J. Southwood (2007), Why does Saturn's auroral oval not respond to the rotating Cam perturbations?, *Eos Trans. AGU*, *88*(52), Fall Meet. Suppl., Abstract P52B–02.

Kurth, W. S., A. Lecacheux, T. F. Averkamp, J. B. Groene, and D. A. Gurnett (2007), A Saturnian longitude system based on a variable kilometric radiation period, *Geophys. Res. Lett.*, *34*, L02201, doi:10.1029/2006GL028336.

Kurth, W. S., T. F. Averkamp, D. Gurnett, J. B. Groene, and A. Lecacheux (2008), An update to a Saturnian longitude system based on kilometric radio emissions, *J. Geophys. Res.*, *113*, A05222, doi:10.1029/2007JA012861.

Lamy, L., P. Zarka, B. Cecconi, R. Prangé, W. S. Kurth, and D. A. Gurnett (2008), Saturn kilometric radiation: Average and statistical properties, *J. Geophys. Res.*, *113*, A07201, doi:10.1029/2007JA012900.

Lecacheux, A., and F. Genova (1983), Source localization of Saturn kilometric radio emission, *J. Geophys. Res.*, *88*, 8993–8998, doi:10.1029/JA088iA11p08993.

Nichols, J. D., and S. W. H. Cowley (2004), Magnetosphere-ionosphere coupling currents in Jupiter's middle magnetosphere: Effect of precipitation-induced enhancements of the Pedersen conductivity, *Ann. Geophys.*, *22*, 1799–1827.

Press, W. H., B. P. Flannery, S. A. Teukolsky, and W. T. Vetterling (2007), *Numerical Recipes in C: The Art of Scientific Computing*, 3rd ed., pp. 685–692, Cambridge Univ. Press, Cambridge, U.K.

Smith, E. J., L. Davis Jr., D. E. Jones, P. J. Coleman Jr., D. S. Colburn, P. Dyal, and C. P. Sonett (1980), Saturn's magnetosphere and its interaction with the solar wind, *J. Geophys. Res.*, *85*(A11), 5655–5674, doi:10.1029/JA085iA11p05655.

Southwood, D. J., and M. G. Kivelson (2007), Saturnian magnetospheric dynamics: Elucidation of a camshaft model, *J. Geophys. Res.*, *112*, A12222, doi:10.1029/2007JA012254.

Vincent, M. B., et al. (2000), Mapping Jupiter's latitudinal bands and Great Red Spot using HST/WFPC2 far-ultraviolet imaging, *Icarus*, *143*, 189–204, doi:10.1006/icar.1999.6232.

Warwick, J. W., et al. (1981), Planetary radio astronomy observations from Voyager 1 near Saturn, *Science*, *212*, 239–243, doi:10.1126/science.212.4491.239.

Zarka, P., L. Lamy, B. Cecconi, R. Prangé, and H. O. Rucker (2007), Modulation of Saturn's radio clock by solar wind speed, *Nature*, *450*, 265–267, doi:10.1038/nature06237.

J. T. Clarke, J. Duval, and S. Wannawichian, Center for Space Physics, Boston University, 725 Commonwealth Avenue, Boston, MA 02215, USA.

S. W. H. Cowley and J. D. Nichols, Department of Physics and Astronomy, University of Leicester, Leicester LE1 7RH, UK. (jdn@ion.le.ac.uk)

A. J. Farmer, Harvard-Smithsonian Center for Astrophysics, Harvard University, 60 Garden Street, Cambridge, MA 02138, USA.

J.-C. Gérard and D. Grodent, Institut d'Astrophysique et de Géophysique, Université de Liège, Allée du 6 Août, 17, B-4000 Liege, Belgium.